Journal of Materials Chemistry C

ROYAL SOCIETY OF CHEMISTRY

PAPER

View Article Online
View Journal | View Issue

Check for updates

Cite this: J. Mater. Chem. C, 2025, 13, 14061

Janus MoSeS nanoscrolls for ultrasensitive detection of surface-enhanced Raman scattering†

Qixin Deng,[ab] Da Zhan, *[a] Jiaxu Yan,[a] Pengtao Jing,[a] Yang Bao,[a] Jilian Xu,[a] Hai Xu,[a] Binghui Li,[a] Ligong Zhang,[a] Kewei Liu,[a] Lei Liu[a] and Dezhen Shen[a]

Received 20th February 2025, Accepted 24th May 2025

DOI: 10.1039/d5tc00742a

rsc.li/materials-c

Surface-enhanced Raman scattering (SERS) has become an indispensable molecular detection technique due to its exceptional sensitivity and selectivity. However, conventional SERS methods often rely on complex metallic nanostructures, leading to background noise and performance limitations. This study addresses these challenges by investigating the potential of Janus MoSeS nanoscrolls as SERS substrates based on a chemical enhancement mechanism to achieve ultrasensitive detection. We employed a room-temperature plasma-assisted method to synthesize Janus MoSeS, followed by the formation of nanoscroll structures to enhance Raman signal intensity. Comparative SERS experiments revealed that Janus MoSeS nanoscrolls significantly outperformed defective $MoSe_2$, achieving enhancement factors of 8.04×10^{11} for rhodamine 6G (R6G), 1.14×10^{7} for methylene blue (MB) and 2.12×10^{8} for crystal violet (CV) detection. Findings indicate that the unique dipole orientation of Janus TMDs contributes to enhanced SERS performance, while the nanoscroll architecture maximizes the effective interaction area with probe molecules. This research presents an approach for developing metal nanoparticle-free, non-plasmonic SERS substrates, thereby advancing the field of excitonic SERS technologies.

1. Introduction

Driven by the enhancement of molecular vibrational modes upon interaction with substrates, surface-enhanced Raman scattering (SERS) has emerged as a crucial molecular detection technique owing to its high sensitivity and selectivity.[1–3] Such enhancements facilitate the detection of molecules at trace levels, including single-molecule detection. The non-destructive nature and rapid detection capabilities of SERS make it valuable for applications such as health monitoring, catalytic process observation, and *in situ* dynamic tracking of molecular interactions.[4–7] SERS enhancement is generally attributed to two mechanisms: electromagnetic (EM) and chemical (CM). The EM mechanism involves the amplification of local electromagnetic fields *via* plasmon excitation, which significantly boosts Raman scattering signals. CM enhancement arises from charge transfer and chemisorption between molecules and substrate. However, despite the substantial signal amplification, EM-based SERS relies on the construction of metallic nanostructures, which are often complex to fabricate and introduce background noise. This challenge has spurred growing interest in exploring non-plasmonic excitonic SERS substrates that do not require metal nanostructures.

Two-dimensional (2D) materials, including graphene, hexagonal boron nitride (h-BN), and transition metal dichalcogenides (TMDs), have attracted significant interest from academia and industry over the past decade owing to their unique electronic, mechanical, chemical, and thermal properties. Numerous studies have reported the applications of various 2D materials in SERS,[8,9] with the mechanisms of Raman enhancement varying across different experimental designs. However, most 2D SERS substrates with high enhancement factors still require metal nanoparticles or nanostructures, limiting their ability to exploit intrinsic properties for cost-effective and high-level Raman enhancement. Recently, both the dipole–dipole interaction mechanism in h-BN[10] and the twisted octahedral structures of 1T′-WTe_2 and 1T′-$MoTe_2$[11] have been used as SERS substrates. Furthermore, monolayer Janus MoSSe, which possesses out-of-plane dipoles, has been confirmed as a viable SERS substrate.[12] The dipoles in the monolayer Janus TMDs originate from different chalcogen atoms on either side of the transition metal layer. However, their impact on Raman enhancement is limited by the small electronegativity difference between the two atoms. Theoretical studies suggest that stacking monolayer Janus TMDs into

[a] State Key Laboratory of Luminescence Science and Technology, Changchun Institute of Optics, Fine Mechanics and Physics, Chinese Academy of Sciences, Changchun, Jilin, 130033, China. E-mail: zhanda@ciomp.ac.cn
[b] University of Chinese Academy of Sciences, Chinese Academy of Sciences, Beijing, 100049, China

† Electronic supplementary information (ESI) available. See DOI: https://doi.org/10.1039/d5tc00742a

multilayers induces charge transfer due to their intrinsic dipoles, leading to a stronger built-in quasi-electric field within the multilayer structure.[13] This theoretical framework offers the potential that Janus TMDs can enhance Raman signals by exploiting their intrinsic properties. However, efficient stacking of multilayer Janus TMDs with clean interfaces remains a significant challenge.

To enhance SERS efficiency by mimicking the effects of multilayer stacking, we first synthesized monolayer Janus MoSeS (JMSS) using a room-temperature plasma-assisted method and then fabricated it into a nanoscroll structure *via* water surface tension. Additionally, we synthesized monolayer defective $MoSe_2$ (DMS) and similarly prepared its nanoscroll for comparative analysis. In this study, a series of SERS experiments were conducted on the aforementioned monolayers and their nanoscrolls. Analysis of the Raman spectra of the tested molecules revealed that the Raman enhancement of the Janus MoSeS nanoscrolls (JMSS-NS) significantly exceeded that of the defective $MoSe_2$ nanoscrolls (DMS-NS), with enhancement factors reaching 8.04×10^{11} for Rhodamine 6G (R6G), 1.14×10^{7} for Methylene Blue (MB) and 2.12×10^{8} for crystal violet (CV) detection, indicating ultrasensitive detection performance. This experimental design not only validates the advantages of Janus TMD nanoscroll structures for SERS applications but also provides new insights into the distinct Raman enhancement mechanisms of Janus TMDs compared with conventional TMDs. These findings are expected to open new ways for designing metal nanoparticle-free nanostructured SERS substrates and for the advancement of non-plasmonic excitonic SERS technologies driven by the intrinsic properties of materials.

2. Methods and characterization

2.1. Synthesis of monolayer pristine CVD $MoSe_2$

Triangular monolayer $MoSe_2$ was synthesized on SiO_2/Si (300 nm) substrates *via* chemical vapor deposition (CVD), using selenium powder as the selenium precursor and MoO_3 as the molybdenum source (Fig. S1, ESI†). A quartz boat containing 5 mg of MoO_3 powder was positioned at the center of the tubular furnace, with a SiO_2/Si substrate carefully placed on top of the powder. The designed temperature of selenium (~240 °C) was controlled by adjusting its distance from the heating center. The furnace temperature was gradually raised to the growth temperature of 800 °C at a rate of 50 °C per minute and held for 10 minutes to facilitate $MoSe_2$ growth with a flow of 40 sccm high-purity argon and 2 sccm high-purity hydrogen. After the reaction, the CVD system was allowed to cool naturally to room temperature.

2.2. Synthesis of monolayer Janus MoSeS

Similar to our previous report,[14] Janus MoSeS was synthesized at room temperature by replacing selenium atoms in the top layer of the CVD-grown monolayer $MoSe_2$ with sulfur atoms. A commercial inductively coupled plasma system with adjustable RF power was used. The system featured a 2-inch quartz tube wrapped with 16 turns of a copper inductor at one end to generate plasma. Then, 300 mg of sulfur powder was placed in a quartz boat upstream of the copper inductor, along with the substrate containing the monolayer $MoSe_2$ sample, located 50 and 38 cm away from the plasma generation center, respectively, as shown in Fig. 1a. Once the system was sealed, a vacuum pump stabilized the pressure inside the quartz tube

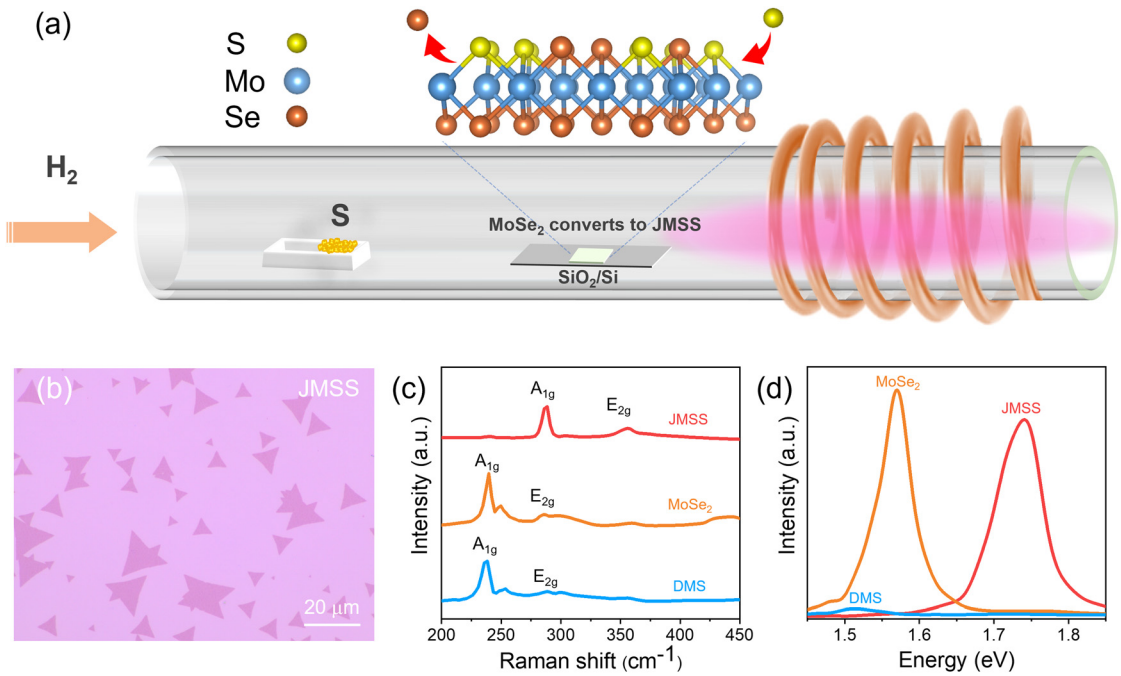

Fig. 1 (a) Schematic of the hydrogen plasma treatment. (b) OM image of the obtained JMSS. (c) Raman and (d) photoluminescence spectra of JMSS, $MoSe_2$ and DMS.

(acting as the reaction chamber) below 5×10^{-3} mbar. After multiple cycles of inert gas filling and venting, 20 sccm of hydrogen was introduced, and the chamber pressure was maintained at approximately 300 mbar. Hydrogen plasma was excited using 15 W RF power, causing sulfur powder to interact with the plasma and form various reactive radicals and charged species. These species disrupted the Mo–Se bonds in the upper layer of $MoSe_2$, facilitating the formation of Mo–S bonds. Finally, the Mo–Se bonds in the upper layer were replaced with Mo–S bonds, thereby completing the conversion from monolayer $MoSe_2$ to Janus MoSeS.

2.3. Synthesis of 2D material nanoscrolls

To avoid interference from impurity signals during the SERS test, the preparation of 2D material nanoscrolls in this experiment followed a solvent-free curling method reported by Zhao *et al.*[15] First, the grown 2D materials were heated on a hot stage at 80–100 °C for approximately 10 minutes. Then, 3 μL of deionized water was dispensed onto one side of the substrate using a pipette, and a coverslip was used to slowly drag the water droplets across the surface. This process uses the surface tension of water to transform 2D flakes into nanoscrolls. The process of preparing nanoscrolls and the corresponding optical and SEM images are shown in Fig. S2 (ESI†). In particular, during the fabrication of Janus TMDs nanoscrolls, the curling tendency predominantly occurs toward the side with atoms of smaller Bohr radius,[16,17] meaning that when S atoms occupy the upper layer of the Janus structure, they facilitate the formation of stable nanoscroll configurations with S atoms facing inside. Thus, $MoSe_2$ was selected as the precursor to sulfurize the upper Se layer, forming the S–Mo–Se structure from the upper surface to the bottom surface, and the Se layer is kept in contact with the substrate, which facilitates the formation of nanoscrolls with the S and Se atom layers facing inside and outside, respectively.

2.4. SERS measurements

Solutions of R6G with concentrations ranging from 10^{-8} to 10^{-15} M and MB with concentrations ranging from 10^{-6} to 10^{-11} M were prepared as probe molecules for later SERS measurements. The prepared 2D flakes and nanoscrolls were used as SERS substrates and immersed in the solutions for 30 minutes to achieve the adsorption of probe molecules on the surface. The SERS substrates were then removed from the solutions and immediately dried using a nitrogen gun. To maximize the adsorption of probe molecules on the SERS substrate, intercalated-nanoscrolls of the probe molecules were prepared, which required the adsorption of probe molecules on 2D flakes, followed by encapsulation of the molecules inside the interlayer spaces of the nanoscrolls (Fig. 3a, see Section 2.3 for details). The SERS tests were performed using a 532 nm laser as the excitation source, and the data acquisition process was conducted with a laser power of 0.5 mW. The spectrometer acquired Raman spectra for 30 seconds using a 600 gr mm^{-1} grating.

3. Results and discussion

3.1. Characterization of SERS substrates

Monolayer $MoSe_2$ was synthesized using a traditional CVD method. Using $MoSe_2$ as a precursor, JMSS was subsequently prepared by plasma-assisted deposition (Fig. 1a), and DMS was obtained by surface plasma irradiation.[18] Fig. 1b shows an optical microscope (OM) image of JMSS, which exhibits a morphology similar to that of pristine $MoSe_2$ and DMS (Fig. S3, ESI†). However, the Raman spectra (Fig. 1c) show a significant difference between pristine $MoSe_2$, DMS, and JMSS. The plasma irradiation-induced lattice distortions and defects (DMS) only give a slight redshift and broadening of the typical A_{1g} and E_{2g} Raman peaks compared to those of the pristine $MoSe_2$, while these two peaks exhibit a blueshift after conversion to JMSS. Raman spectroscopy is a sensitive probe of atomic vibrational modes, particularly in revealing structural modifications. In samples with incomplete substitution, residual $MoSe_2$ domains (where Mo atoms remain coordinated by Se atoms on both sides) exhibit characteristic $MoSe_2$ Raman peaks at $\sim$240 cm^{-1}. For the JMSS sample, these diagnostic peaks disappeared, as shown by the red curve in Fig. 1c. Furthermore, no Raman signatures corresponding to partially upper and lower atomic layer substituted $MoS_{2x}Se_{2(1-x)}$ alloys[19] appeared in the Raman spectra of Janus MoSeS. The observed Raman shift positions, combined with the photoluminescence spectroscopy (PL) spectra (Fig. 1d) features, align precisely with previously reported Janus MoSeS structures.[12,14] These collective findings confirm the near-complete substitution of upper Se atoms with S in $MoSe_2$, resulting in the formation of JMSS.

The PL spectra of JMSS, $MoSe_2$, and DMS are shown in Fig. 1d. The peak of DMS was significantly weaker, with its peak position slightly redshifted compared to that of pristine $MoSe_2$, indicating that a substantial number of defects had been introduced into DMS. On the other hand, the PL peak position of pristine $MoSe_2$ undergoes a significant blueshift from 1.57 eV to 1.74 eV after conversion to JMSS by plasma-assisted treatment, which is due to the obvious increase in the energy bandgap. It should be noted that the PL peak of JMSS only shows a slight decrease in intensity and a minor broadening in full width at half maximum (FWHM) compared with those of pristine $MoSe_2$, suggesting that the prepared JMSS is highly crystalized and exhibits significantly fewer defects than DMS.

3.2. SERS performance of 2D flakes

Janus TMDs naturally possess dipoles oriented perpendicular to the basal plane because of the different chalcogen atoms (sulfur and selenium) on each side of the transition metal layer. This crystallographic feature, which induces such a physical property, represents the most significant distinction between Janus TMD flakes and conventional TMD flakes. According to the theory of SERS enhancement, Janus TMD flakes driven by these vertical dipoles, as depicted in Fig. 2a, are expected to exhibit superior SERS enhancement compared to conventional TMDs. To investigate this, Raman spectra were acquired from the probe molecules adsorbed on three different 2D flakes

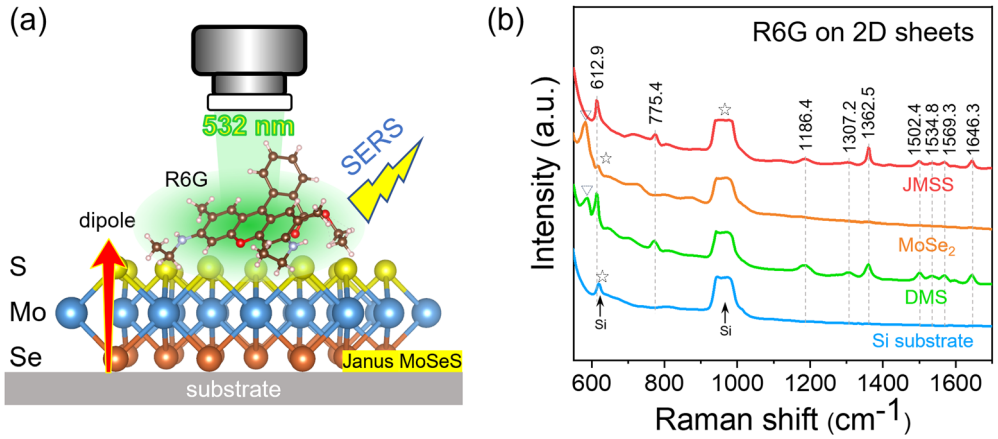

Fig. 2 (a) SERS mechanism of monolayer Janus materials. (b) Raman spectra of R6G molecules (10^{-8} M) on different 2D flakes and SiO_2/Si.

(denoted as JMSS-F, $MoSe_2$-F, and DMS-F, respectively) synthesized on SiO_2/Si substrates (see Section 3.1).

Using R6G at a concentration of 10^{-8} M as the probe molecule, the SERS performance of these three distinct 2D flakes is presented in the Raman spectra (Fig. 2b). The Raman signals of R6G are almost undetectable on the pristine monolayer $MoSe_2$ and bare SiO_2/Si substrates, whereas both monolayer JMSS and DMS exhibit strong Raman signals with minimal difference in intensity. Although the Raman signals of R6G molecules detected on JMSS-F and DMS-F were comparable, the mechanisms underlying SERS enhancement are different. The SERS mechanism of DMS primarily originates from the generation of local dipoles and suppression of R6G fluorescence due to photogenerated charge transfer between R6G molecules and the sample.[18,20] In contrast, the enhancement effect of JMSS mainly arises from the out-of-plane dipoles induced by the natural S–Mo–Se structure, which are distributed across the entire basal plane. This can probably be attributed to the relatively weak dipole moment of the monolayer JMSS, which could explain why its Raman enhancement signal for R6G was not significantly stronger than that of DMS. To verify this hypothesis and to further improve the SERS enhancement of JMSS, the nanoscroll structures of both materials were prepared for subsequent SERS measurements and analysis.

3.3. SERS performance of the Janus MoSeS nanoscrolls

JMSS-NS and DMS-NS were prepared following the method outlined in Section 2.3. The preparation process is illustrated by the orange arrows in Fig. 3a. To ensure experimental consistency, the concentration of the R6G solution used during immersion was maintained at the same level as that of the JMSS-F (10^{-8} M). The green and blue curves in Fig. 3b represent the Raman spectra of R6G molecules adsorbed on the JMSS-NS and DMS-NS SERS substrates, respectively. The intensity of the R6G Raman peaks indicates that compared with JMSS-F, the Raman signal of R6G molecules is enhanced when adsorbed on the outer surface of JMSS-NS (Fig. S4a, ESI†), which may be attributed to the curling behaviour. In contrast, DMS-NS not only failed to enhance the R6G signal but exhibited a lower intensity than the DMS-F (Fig. S4b, ESI†).

To ensure the general reliability of the relative magnitudes of the Raman signal intensities measured on the curled SERS substrates, 20 sets of Raman spectra were collected for JMSS-NS and DMS-NS, respectively. The intensity of the R6G Raman peak at 1361.1 cm^{-1} of each spectrum was selected as a reference value and plotted as shown by the green and blue circles in Fig. 3c. The average intensity of the R6G Raman signals enhanced by JMSS-NS is greater than that enhanced by DMS-NS, confirming the reliability of the result and highlighting the differences in the SERS enhancement mechanisms between JMSS-F and DMS-F. According to the literature, when multiple monolayers of JMSS stack to form a multilayer structure, the intrinsic dipole of multilayered JMSS induces a stronger built-in quasi-electric field in the multilayer structure.[13] When the JMSS is formed into a nanoscroll structure, it is analogous to concentric stacking, with the nanoscroll axis as the center, generating a stronger built-in quasi-electric field. This stronger built-in quasi-electric field will enhance charge transfer between JMSS-NS and R6G molecules and cause greater SERS performance compared to that of the monolayer JMSS (Fig. 3a). Consequently, when acting as a SERS substrate, JMSS-NS provides further enhancement of the Raman signal compared with JMSS-F. In contrast to DMS-NS, the local dipoles generated in the inner defective layers of the nanoscrolls have limited interaction with the probe molecules adsorbed on the outer surface. Instead, only the local dipoles generated by the defects in the outer layer dominate the interaction with the adsorbed probe molecules, resulting in a suboptimal SERS effect.

Although JMSS-NS had a much better SERS effect than JMSS-F, it should be noted that the R6G molecules could only be adsorbed onto the outer surface of the nanoscrolls during immersion, which severely limited the number of R6G molecules that could be adsorbable due to the restricted outer surface area. To further enhance the capability of the nanoscroll-like SERS substrate for detecting the limit of the probe molecule concentration, probe molecule intercalated-nanoscrolls were

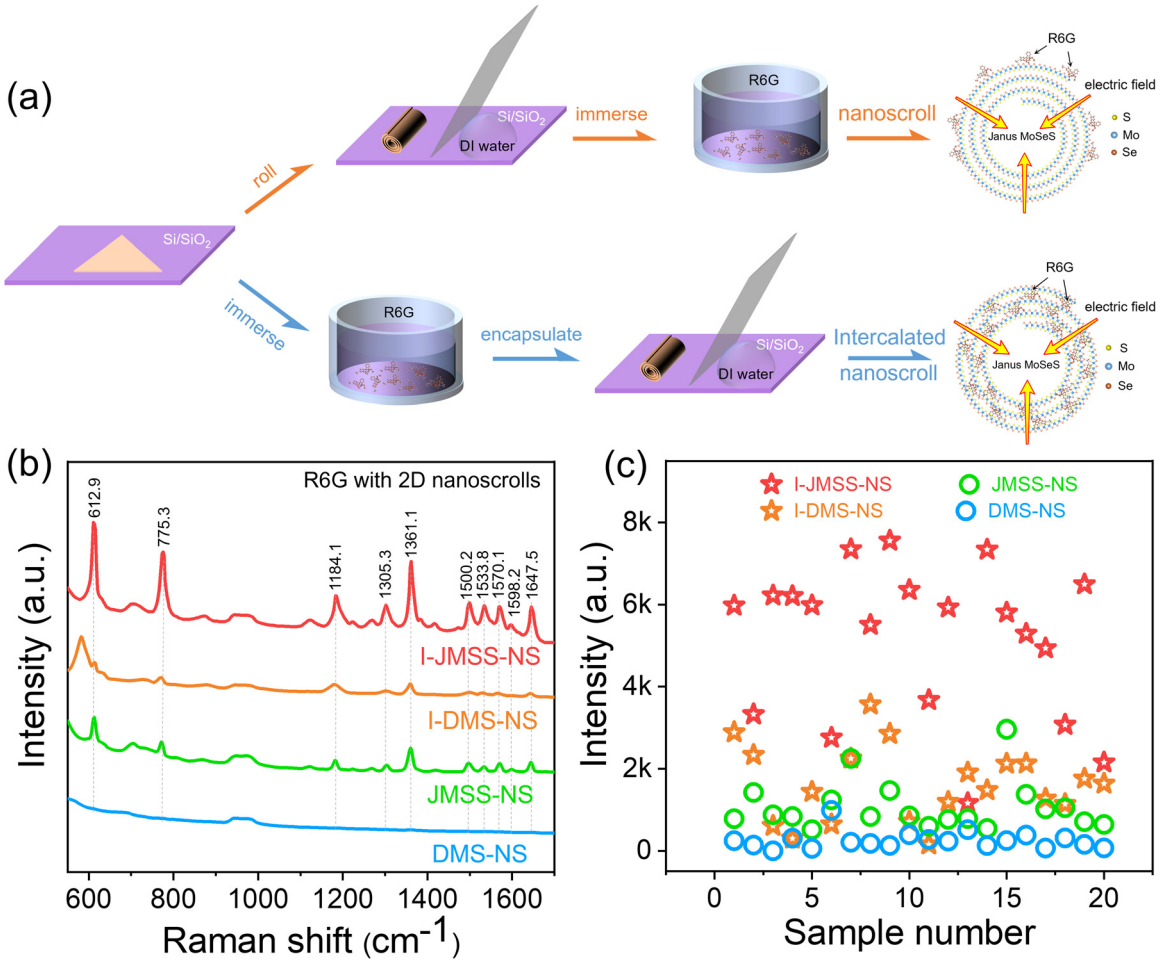

Fig. 3 (a) Adsorption processes of R6G molecules on the outer surface of the nanoscroll (orange-arrow route) and encapsulation processes of R6G molecules on the inner surface of the nanoscroll (blue-arrow route). (b) Raman spectra of R6G molecules (10^{-8} M) with different 2D nanoscrolls. (c) Statistical plot of Raman intensity for the 1361.1 cm^{-1} vibrational mode of R6G molecules with different 2D nanoscrolls.

prepared, and the preparation process is schematically shown by the blue arrows in Fig. 3a. Notably, the Raman focusing detection area on the intercalated-nanoscroll contains a significantly higher density of probe molecules. This is because, in addition to the molecules adsorbed on the outer surface of the scroll structure, the space between the internal stacking layers is fully utilized to encapsulate additional probe molecules.

The Raman spectra of intercalated-Janus MoSeS nanoscrolls (I-JMSS-NS) and intercalated-defective $MoSe_2$ nanoscrolls (I-DMS-NS) are shown in red and orange curves in Fig. 3b. The Raman signals of R6G are further enhanced in I-JMSS-NS compared to JMSS-NS (green curve). Additionally, the intensity of the Raman peaks for R6G was also enhanced in I-DMS-NS, although it remained weaker than that in I-JMSS-NS. To verify the reliability of this conclusion, 20 sets of SERS spectra from I-JMSS-NS and I-DMS-NS were collected, and the intensity of the R6G Raman peak at 1361.1 cm^{-1} in each spectrum was used as a reference and plotted as red and orange pentagrams, respectively (Fig. 3c). The average intensity of the R6G Raman signals detected on the I-JMSS-NS was significantly higher than that detected on the I-DMS-NS. In addition to the stronger effect induced by the built-in quasi-electric field of JMSS-NS, encapsulating probe molecules within I-JMSS-NS takes full advantage of the inner surface space of the nanoscroll structure, effectively increasing the detectable R6G molecular density. These synergistic effects further enhanced the Raman signals of the probe molecules. For I-DMS-NS, the encapsulation also increases the number of R6G molecules, but because of the absence of a built-in quasi-electric field, its SERS enhancement effect remained lower than that of I-JMSS-NS.

To confirm the charge-transfer mechanism of these SERS substrates, PL spectroscopy was performed on JMSS-F and JMSS-NS, both with and without adsorbed probe molecules (Fig. 4). The PL intensity of JMSS-F adsorbed with the R6G molecules is significantly reduced, with the peak position red-shifted in Fig. 4a. This phenomenon is commonly observed due to charge transfer-induced electron doping in TMDs, causing a lower exciton/trion ratio to decrease the PL peak intensity and shifting it to a lower energy.[21–23] Thus, changes in the PL intensity and position of JMSS can be caused by charge transfer between R6G and JMSS-F. The PL peak of JMSS-NS (Fig. S5, ESI†) exhibited

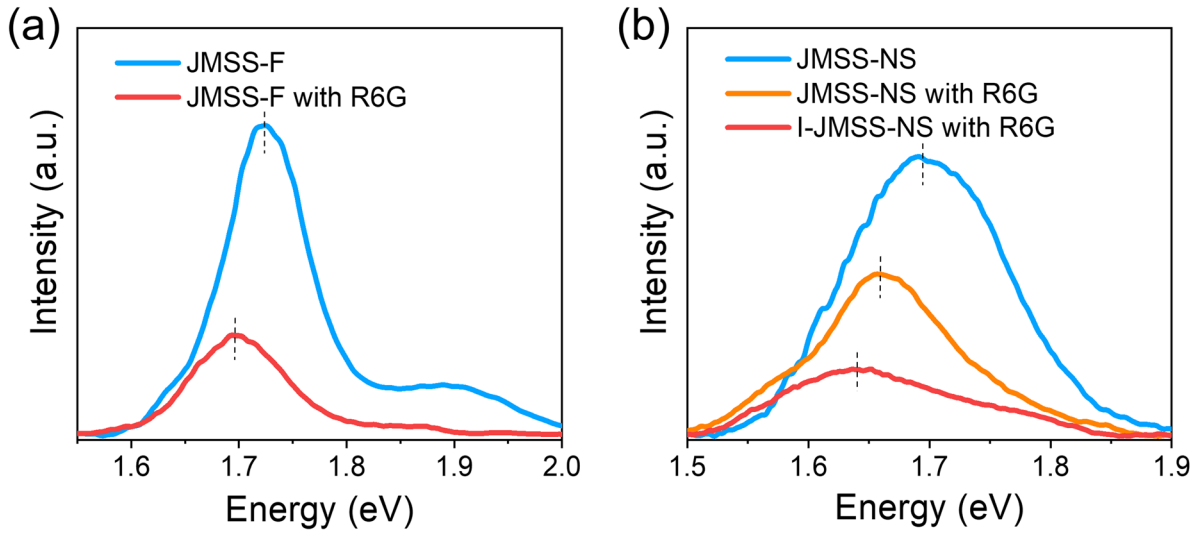

Fig. 4 PL spectra of (a) JMSS-F and (b) JMSS-NS with and without R6G.

a redshift and a substantial reduction in intensity compared with that of JMSS-F, which is consistent with previously reported results.[16,17] After adsorption of R6G molecules, the PL of I-JMSS-NS exhibited further attenuation and redshift (Fig. 4b). This phenomenon is probably attributed to the enhanced charge transfer in I-JMSS-NS driven by the built-in quasi-electric field, which also makes a synergistic contribution together with the higher spatial density of R6G molecules formed by the interlayer insertion in the scrolled multi-layer structure of JMSS-NS, thus dramatically improving the SERS performance of I-JMSS-NS.

3.4. Ultra-sensitive detection of probe molecules in intercalated-Janus MoSeS nanoscrolls

To quantify the detection capability of I-JMSS-NS, we systematically investigated its sensitivity and enhancement factors for both R6G and MB molecules. The Raman spectra of I-JMSS-NS at various concentrations of R6G solutions are presented in Fig. 5a. As the concentration of the solution decreases, fewer R6G molecules are encapsulated within the nanoscrolls, leading to a continuous reduction in the intensity of the Raman peaks, with some peaks becoming undetectable. When the solution concentration was reduced to 10^{-15} M, the most pronounced vibrational mode at 1361.2 cm^{-1} of R6G remained detectable, showing an extremely low concentration detection capability. To demonstrate the broad applicability of I-JMSS-NS to other SERS molecules, MB was also used as the probe molecule for further SERS measurements (Fig. 5b). MB exhibited strong characteristic Raman peaks upon adsorption on I-JMSS-NS at a concentration of 10^{-5} M. The intensities of the MB Raman peaks gradually decreased with decreasing MB concentration, and the peak at 1622.7 cm^{-1} can also be detected even at concentrations as low as 10^{-11} M. Furthermore, the Raman spectra of CV molecules with different concentrations are shown in Fig. S6 (ESI†). It can be seen that even a concentration as low as 10^{-11} M can be detected.

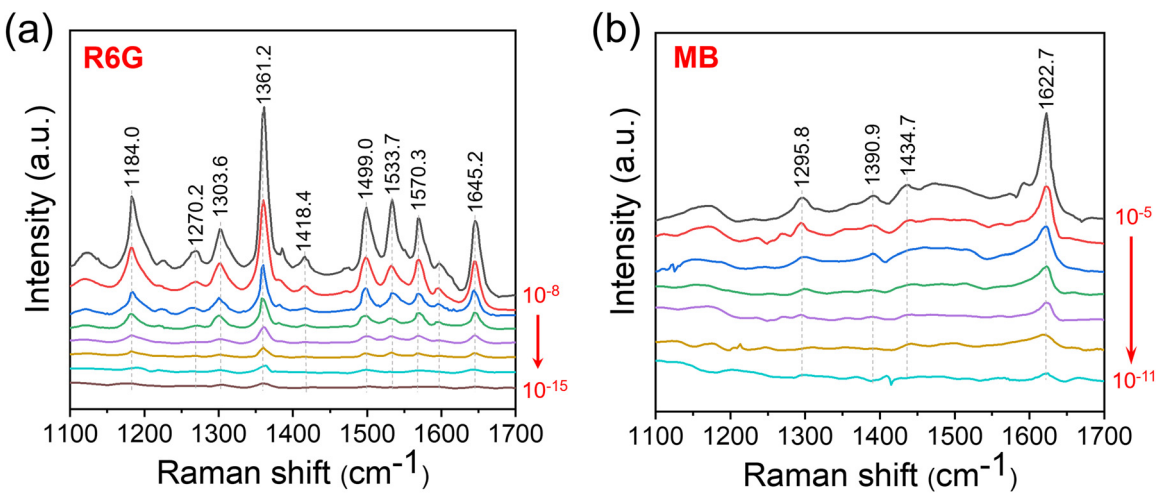

Fig. 5 Raman spectra of (a) R6G and (b) MB molecules at different concentrations in I-JMSS-NS.

The SERS enhancement factor (EF) represents the ratio of the Raman signals of the probe molecules with and without the influence of the SERS substrate:

$$\mathrm{EF} = \frac{I_{\mathrm{SERS}} N_{\mathrm{RS}}}{I_{\mathrm{RS}} N_{\mathrm{SERS}}}$$

where I_{SERS} and I_{RS} represent the Raman intensities of the probe molecules adsorbed on the SERS substrate and the SERS-free substrate, respectively, and N_{SERS} and N_{RS} represent the number of probe molecules on the SERS substrate and the SERS-free substrate, respectively. Based on the data in Fig. 5, the EFs of R6G MB and CV molecules encapsulated in I-JMSS-NS were calculated to be 8.04×10^{11}, 1.14×10^{7} and 2.12×10^{8}, respectively, which are comparable to recent reports using metal nanoparticle-free SERS substrates (Table S1, ESI†).[24–28]

4. Conclusions

In this study, monolayer JMSS and DMS were successfully synthesized, and their respective nanoscroll structures were further fabricated to investigate their SERS performance. Through a series of SERS experiments using R6G and MB as probe molecules, we observed that JMSS-NS exhibited a significantly higher Raman enhancement than JMSS-F and DMS-NS. This enhancement is attributed to the amplification of intrinsic out-of-plane dipoles in JMSS-NS, which is driven by the stronger built-in quasi-electric field induced by the multilayer stacking effect *via* curling the flake to form nanoscrolls. Furthermore, by designing and experimentally constructing a novel structure in which the 2D-JMSS surface pre-adsorbed with probe molecules is curled to form intercalated-nanoscrolls (I-JMSS-NS), the adsorption of probe molecules is maximized. The formation of the I-JMSS-NS structure effectively increased the number of detected molecules. Thus, these two synergistic effects effectively enhance the SERS detection sensitivity for low-concentration molecules, resulting in an ultrasensitive detection limit as low as 10^{-15} M for R6G and 10^{-11} M for MB and CV. These findings demonstrate that metal nanoparticle-free JMSS-NS can achieve significant Raman signal enhancement without the need for metal nanostructure-assisted hybridization, highlighting their potential as non-plasmonic SERS substrates for ultrasensitive detection. This study not only highlights the advantages of Janus TMDs-based nanoscroll structures in SERS applications through their novel structural design but also offers new insights into advancing non-plasmon excitonic SERS technology by utilizing intrinsic dipoles in two-dimensional materials. In particular, integrating the highly sensitive molecular detection capabilities of such biocompatible I-JMSS-NS SERS substrates with the specific identification of biological targets (*e.g.*, proteins, DNA, pathogens, or cells) will be crucial for future applications in biomolecular detection.

Author contributions

QiXin Deng: writing, review and editing, writing – original draft, investigation, data curation, formal analysis, methodology, and conceptualization. Da Zhan: writing, reviewing, editing, investigation, and supervision. Jiaxu Yan: investigation and supervision. Pengtao Jing: investigation. Yang Bao: investigation. Jilian Xu: investigation. Hai Xu: investigation. Binghui Li: investigation. Ligong Zhang: investigation. Kewei Liu: investigation. Lei Liu: project administration, resources, and funding acquisition. Dezhen Shen: project administration, resources, and funding acquisition.

Data availability

The authors confirm that the data supporting the findings of this study are available within the article.

Conflicts of interest

The authors declare that they have no known competing financial interests or personal relationships that could have appeared to influence the work reported in this paper.

Acknowledgements

This work was supported by the National Natural Science Foundation of China, China (Grant number: 11727902, 12074372, 12174385, 62074148), and the 100 Talents Program of the Chinese Academy of Sciences, China.

References

1 X. X. Han, R. S. Rodriguez, C. L. Haynes, Y. Ozaki and B. Zhao, *Nat. Rev. Methods Primer*, 2022, **1**, 87.
2 C. Li, Y. Huang, X. Li, Y. Zhang, Q. Chen, Z. Ye, Z. Alqarni, S. E. J. Bell and Y. Xu, *J. Mater. Chem. C*, 2021, **9**, 11517–11552.
3 J. Langer, D. Jimenez de Aberasturi, J. Aizpurua, R. A. Alvarez-Puebla, B. Auguié, J. J. Baumberg, G. C. Bazan, S. E. J. Bell, A. Boisen, A. G. Brolo, J. Choo, D. Cialla-May, V. Deckert, L. Fabris, K. Faulds, F. J. García de Abajo, R. Goodacre, D. Graham, A. J. Haes, C. L. Haynes, C. Huck, T. Itoh, M. Käll, J. Kneipp, N. A. Kotov, H. Kuang, E. C. Le Ru, H. K. Lee, J.-F. Li, X. Y. Ling, S. A. Maier, T. Mayerhöfer, M. Moskovits, K. Murakoshi, J.-M. Nam, S. Nie, Y. Ozaki, I. Pastoriza-Santos, J. Perez-Juste, J. Popp, A. Pucci, S. Reich, B. Ren, G. C. Schatz, T. Shegai, S. Schlücker, L.-L. Tay, K. G. Thomas, Z.-Q. Tian, R. P. Van Duyne, T. Vo-Dinh, Y. Wang, K. A. Willets, C. Xu, H. Xu, Y. Xu, Y. S. Yamamoto, B. Zhao and L. M. Liz-Marzán, *ACS Nano*, 2020, **14**, 28–117.
4 X. Zheng, Z. Ye, Z. Akmal, C. He, J. Zhang and L. Wang, *Chem. Soc. Rev.*, 2024, **53**, 656–683.
5 Z. Sun, X. Ji, S. Lu and J. Du, *J. Environ. Sci.*, 2024, S1001074224004273.

6 X. Huang, B. Sheng, H. Tian, Q. Chen, Y. Yang, B. Bui, J. Pi, H. Cai, S. Chen, J. Zhang, W. Chen, H. Zhou and P. Sun, *Acta Pharm. Sin. B*, 2023, **13**, 1303–1317.
7 L. Ma, M. Liu, X. Zhou, C. Li and T. Wang, *Mater. Chem. Front.*, 2023, **7**, 4880–4899.
8 W. Zhang, Y. Peng, C. Lin, M. Xu, S. Zhao, T. Masaki and Y. Yang, *Surf. Sci. Technol.*, 2024, **2**, 14.
9 J. Jin, Z. Guo, D. Fan and B. Zhao, *Mater. Horiz.*, 2023, **10**, 1087–1104.
10 X. Ling, W. Fang, Y.-H. Lee, P. T. Araujo, X. Zhang, J. F. Rodriguez-Nieva, Y. Lin, J. Zhang, J. Kong and M. S. Dresselhaus, *Nano Lett.*, 2014, **14**, 3033–3040.
11 L. Tao, K. Chen, Z. Chen, C. Cong, C. Qiu, J. Chen, X. Wang, H. Chen, T. Yu, W. Xie, S. Deng and J.-B. Xu, *J. Am. Chem. Soc.*, 2018, **140**, 8696–8704.
12 S. Jia, A. Bandyopadhyay, H. Kumar, J. Zhang, W. Wang, T. Zhai, V. B. Shenoy and J. Lou, *Nanoscale*, 2020, **12**, 10723–10729.
13 A. C. Riis-Jensen, M. Pandey and K. S. Thygesen, *J. Phys. Chem. C*, 2018, **122**, 24520–24526.
14 Q. Deng, G. Chen, Z. Duan, S. Liu, D. Zhan, J. Yan, P. Jing, Y. Bao, J. Xu, H. Xu, B. Li, J. Liu, L. Zhang, K. Liu, L. Liu and D. Shen, *Appl. Surf. Sci.*, 2025, **688**, 162356.
15 Y. Zhao, H. You, X. Li, C. Pei, X. Huang and H. Li, *ACS Appl. Mater. Interfaces*, 2022, **14**, 9515–9524.
16 M. Kaneda, W. Zhang, Z. Liu, Y. Gao, M. Maruyama, Y. Nakanishi, H. Nakajo, S. Aoki, K. Honda, T. Ogawa, K. Hashimoto, T. Endo, K. Aso, T. Chen, Y. Oshima, Y. Yamada-Takamura, Y. Takahashi, S. Okada, T. Kato and Y. Miyata, *ACS Nano*, 2024, **18**, 2772–2781.
17 M. Sayyad, Y. Qin, J. Kopaczek, A. Gupta, N. Patoary, S. Sinha, E. Benard, A. Davis, K. Yumigeta, C.-L. Wu, H. Li, S. Yang, I. S. Esqueda, A. Singh and S. Tongay, *Adv. Funct. Mater.*, 2023, **33**, 2303526.
18 L. Sun, H. Hu, D. Zhan, J. Yan, L. Liu, J. S. Teguh, E. K. L. Yeow, P. S. Lee and Z. Shen, *Small*, 2014, **10**, 1090–1095.
19 H. Li, X. Duan, X. Wu, X. Zhuang, H. Zhou, Q. Zhang, X. Zhu, W. Hu, P. Ren, P. Guo, L. Ma, X. Fan, X. Wang, J. Xu, A. Pan and X. Duan, *J. Am. Chem. Soc.*, 2014, **136**, 3756–3759.
20 X. Fu, H. Wu, Z. Liu, P. Wang, J. Rong, F. Fu, Z. Lin and Y. Dong, *ACS Appl. Nano Mater.*, 2024, **7**, 3988–3996.
21 H. Nan, Z. Wang, W. Wang, Z. Liang, Y. Lu, Q. Chen, D. He, P. Tan, F. Miao, X. Wang, J. Wang and Z. Ni, *ACS Nano*, 2014, **8**, 5738–5745.
22 D. Yan, W. Qiu, X. Chen, L. Liu, Y. Lai, Z. Meng, J. Song, Y. Liu, X.-Y. Liu and D. Zhan, *J. Phys. Chem. C*, 2018, **122**, 14467–14473.
23 K. An, M. Chen, B. He, H. Ai, W. Wang, Z. Zhang, Z. Pan, S. Chen, W. F. Ip, K. H. Lo, J. Chai, S. Wang, M. Yang, S. Wang and H. Pan, *Adv. Mater. Technol.*, 2022, **7**, 2200217.
24 Q. Lv, J. Tan, Z. Wang, P. Gu, H. Liu, L. Yu, Y. Wei, L. Gan, B. Liu, J. Li, F. Kang, H.-M. Cheng, Q. Xiong and R. Lv, *Nat. Commun.*, 2023, **14**, 2717.
25 R. Wang, J. Ma, X. Dai, Y. Gao, C. Gu and T. Jiang, *Sens. Actuators, B*, 2023, **374**, 132782.
26 R. Su, S. Yang, D. Han, M. Hu, Y. Liu, J. Yang and M. Gao, *J. Colloid Interface Sci.*, 2023, **635**, 1–11.
27 T. Jena, M. T. Hossain, U. Nath, M. Sarma, H. Sugimoto, M. Fujii and P. K. Giri, *Npj 2D Mater. Appl.*, 2023, **7**, 8.
28 H. Qiu, M. Wang, L. Zhang, M. Cao, Y. Ji, S. Kou, J. Dou, X. Sun and Z. Yang, *Sens. Actuators, B*, 2020, **320**, 128445.

